Provided for non-commercial research and education use.
Not for reproduction, distribution or commercial use.

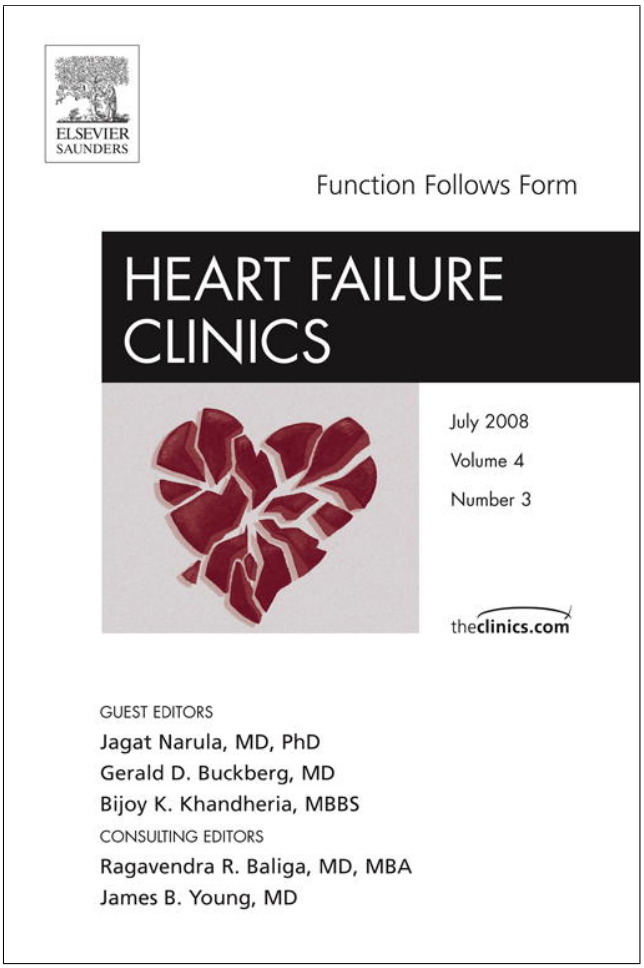

This article appeared in a journal published by Elsevier. The attached copy is furnished to the author for internal non-commercial research and education use, including for instruction at the authors institution and sharing with colleagues.

Other uses, including reproduction and distribution, or selling or licensing copies, or posting to personal, institutional or third party websites are prohibited.

In most cases authors are permitted to post their version of the article (e.g. in Word or Tex form) to their personal website or institutional repository. Authors requiring further information regarding Elsevier's archiving and manuscript policies are encouraged to visit:

http://www.elsevier.com/copyright

Author's personal copy

ELSEVIER
SAUNDERS

Heart Failure Clin 4 (2008) 289–301

HEART
FAILURE
CLINICS

Toward Patient-Specific Myocardial Models of the Heart

Maxime Sermesant, PhD[a,b,*], Jean-Marc Peyrat, MSc[a], Phani Chinchapatnam, PhD[c], Florence Billet, MSc[a], Tommaso Mansi, MSc[a], Kawal Rhode, PhD[b], Hervé Delingette, PhD[a], Reza Razavi, MD[b], Nicholas Ayache, PhD[a]

[a]*Institut National de Recherche en Informatique et en Automatique, Sophia Antipolis, France*
[b]*St Thomas' Hospital, London, UK*
[c]*University College London, London, UK*

Integrating computational models of the heart with clinical data can open up ways to improve diagnosis, treatment planning, and interventions for cardiovascular diseases. It provides a consistent, biophysically based framework for the integration of the fragmented and heterogeneous clinical data currently available. Obtaining patient-specific computational models of the cardiac physiology could help diagnosis by providing physically meaningful cardiac indices. Moreover, once validated, models can have a predictive use and guide in patient management and therapy planning. For example, these computational models provide an excellent basis to optimize the design of implantable devices for improved therapy. However, the application of this modeling research has yet to be translated into the clinical environment, mainly because of the difficulty of validating these models with in vivo data, and efficiently personalizing them.

There is a growing body of literature on the functional imaging of the heart, for example with the measurement of electrical activity, deformation, flows, fiber orientation [1–4], and on the modeling of the electrical and mechanical activity of the heart [5–9]. Many of these models are direct computational models, designed to reproduce in a realistic manner cardiac activity, often requiring high computational costs and the manual tuning of a very large set of parameters.

The proposed approach is to design models that are directly related to the phenomena observed in clinical data. Although the models used here are often simplified when compared with the very detailed models available in the literature, the authors try to select a level of modeling compatible with reasonable computing times and involving a limited number of parameters, thus allowing the identification of the model parameters from clinical measurements of a specific patient, through the resolution of the inverse problem (Fig. 1).

There are still many challenges in achieving a patient-specific electromechanical model of the heart, but some parts can already be personalized, as demonstrated here. The authors will present this work in three sections concerning the anatomy, the electrophysiology, and the biomechanics. But the first challenge in this area is to obtain patient data on these different parts, and integrate them in the same spatio-temporal coordinates.

Clinical data acquisition and fusion

The construction, testing, and personalization of biophysical models rely on the ability to fuse

* Corresponding author. INRIA, Asclepios project, 2004 route des Lucioles, 06 902 Sophia Antipolis, France.
E-mail address: maxime.sermesant@inria.fr (M. Sermesant).

1551-7136/08/$ - see front matter © 2008 Elsevier Inc. All rights reserved.
doi:10.1016/j.hfc.2008.02.014

Author's personal copy

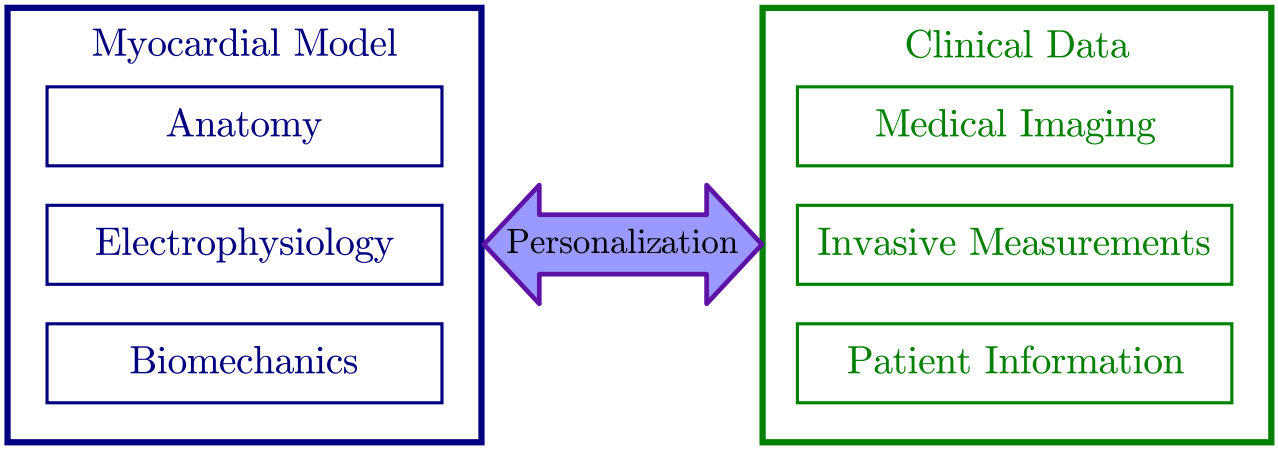

Fig. 1. Global scheme of the model building blocks and of the clinical data used to personalize it.

data from a variety of sources. For cardiac modeling, the fusion of anatomic, mechanical, and electrical data is of primary interest. This fusion must be both in the spatial and temporal domains. High quality cardiac anatomic data can be obtained from both computerized tomography (CT) and magnetic resonance imaging (MRI). MRI can also be used to obtain functional data, such as myocardial wall motion and blood flow. Electrical data can be obtained from catheter-based measurements that are guided using X-ray fluoroscopy.

Spatial fusion of these different data requires an effective image registration strategy. The authors' solution has focused on the use of the X-ray/MR (XMR) hybrid imaging system that allows the seamless collection of both MRI and X-ray-based data (Fig. 2). The authors have developed a real-time registration solution [10] that allows the spatial integration of MRI-based anatomic and functional data with X-ray-based catheter data, such as intracardial electrical and pressure signals. For the temporal integration, the electrocardiogram gives information on the heart rhythm that makes possible the synchronization of the different datasets.

Myocardial anatomy

In the authors' approach, only the compact biventricular myocardium is considered. As the valves are not modeled, the papillary muscles are not simulated, and only the atria and arteries as

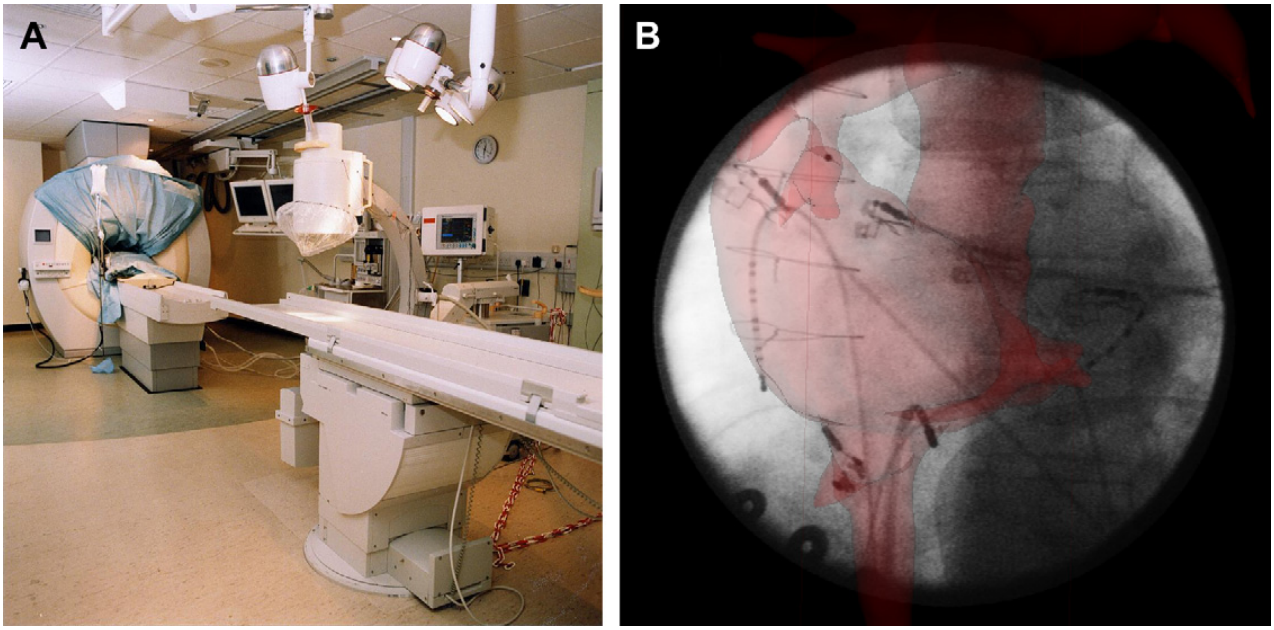

Fig. 2. (*A*) XMR suite with the MR scanner and the X-ray C-arm. (*B*) Catheters in place during an atrial flutter ablation and overlay of the MR-derived anatomy (*in red*) of the right side of the heart.

Author's personal copy

before-load and after-load boundary conditions are integrated.

Patient-specific myocardial shape

The authors have developed a method to create a biventricular mesh adapted to the three-dimensional (3D) image of the heart of a given patient. There is important literature on cardiac image analysis for the segmentation of the heart from medical images [11–21]. The idea is not to be exhaustive but to present a generic pipeline where most of the approaches can fit. The full pipeline relies both on intensity-based algorithms and deformable models [22]. The workflow is to extract from the images a preliminary segmentation of the blood pools and then to adjust the mesh geometry. Deformable models evolve under the influence of both external forces, computed from the preliminary segmentation, and internal forces, computed from the laws of mechanics.

More precisely, the pipeline consists of three main steps, detailed below: image filtering, to enhance image quality and correct possible artifacts; intensity-based labeling, to get a first segmentation of the ventricular cavities; and model-based segmentation, to get the final 3D myocardial shape (Fig. 3).

Image filtering

To increase the robustness of the algorithm on routine cardiac MRI, prone to acquisition artifacts (noise, slice misalignment, motion artifacts), the images must first be processed to facilitate automatic labeling. First, intensity inhomogeneities caused by magnetic field variations can be attenuated using, for instance, the N3 algorithm [23], which estimates image intensity variations using a nonparametric approach. Next, a histogram-based algorithm can be applied to enhance image contrast (remove extrema quantiles). Finally, image signal-to-noise ratio can be improved by using anisotropic filtering, where nonlinear partial differential equations (PDE) are used to smooth the noise while preserving the edges [24].

Intensity-based labeling of left and right blood pools

A first extraction of the ventricular blood pools is achieved by relying on a region-growing approach. For each ventricle, the user interactively places a few control points to define the valve annuli and initial seeds inside the cavities. The algorithm automatically expands the seeds, covering the voxels with similar intensities. In order to enforce the right topology, smooth the borders, and propagate along the time sequence, a deformable surface is then used. The Marching Cubes algorithm [25] provides a 3D surface representing the preliminary segmentation. Then the endocardial surfaces can be extracted from each image of the sequence: the mesh is immersed into the second frame and forces are applied to deform it toward the new endocardial boundaries [13]. An internal force ensures its smoothness while a region-based external force makes it evolve according to the image gray-level intensities. Afterward, the resulting surface is embedded into the following frame and deformed, and so forth until the end of the sequence. Thus, the labeling of both left and right blood pools in each cardiac phase is finally obtained.

Myocardium segmentation

The epicardium is hardly visible in most of the standard clinical MR sequences. Thus, it is first delineated with an interactive tool. The user places a few control points inside, on, and outside the epicardium. A 3D surface is generated in real-time, as the user adds, removes, or moves control points, using variational implicit surfaces and radial basis functions [26]. From the epicardial and endocardial surfaces, a binary image corresponding to the myocardium is created. A volumetric mesh is finally deformed under the influence of internal and external forces. The material properties of the muscle are used in the

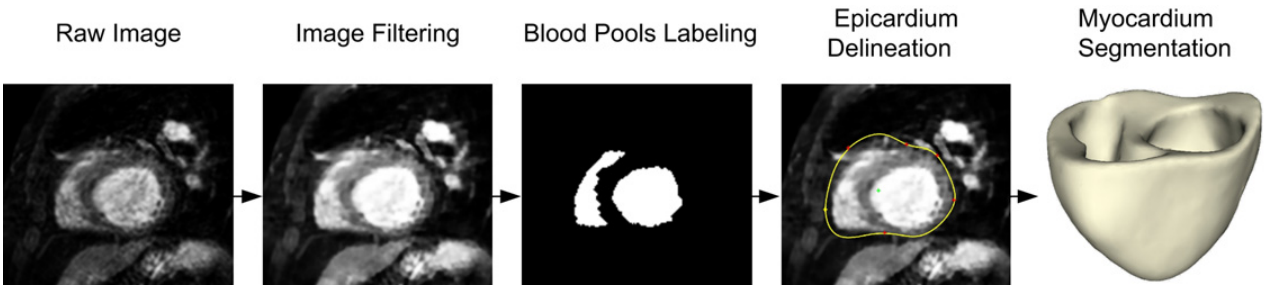

Fig. 3. Global scheme of the segmentation pipeline. Different algorithms can be used for each step of this process.

Author's personal copy

internal forces to ensure the smoothness and the incompressibility of the myocardial mesh [22]. Results of this pipeline are presented in Fig. 4.

Myofiber orientations

In the compact myocardium, the muscle fiber orientations play a crucial role in cardiac electrophysiology and electromechanics. Thus, their introduction in the model is important. However, there is currently no accurate in vivo measurement of these orientations at high resolution [27], so investigators have to mainly rely on prior knowledge.

The complete 3D reconstruction of fiber orientations from histologic sections [28], and more recently its direct 3D acquisition on ex vivo hearts with diffusion tensor MRI (DT-MRI) [29], have been used for a more realistic description of the myofiber architecture. However, they still come from a single subject and thus do not take into account any intersubject variability. In order to improve these models by building an average fiber architecture (Fig. 5) and by measuring its variability, the authors computed a statistical atlas of DT-MRIs from a small database of nine canine hearts [30], which is available on the World Wide Web (http://www-sop.inria.fr/asclepios/data/heart/). The authors performed a groupwise nonrigid registration of the cardiac geometries to an average geometry (see Fig. 5A). Then the DT-MRIs were properly transformed to fit the average geometry in which the average (see Fig. 5B) and covariance of diffusion tensors at each voxel was computed.

Because there is a direct link between the fiber orientations and the primary eigenvector of diffusion tensors, the authors derived the fiber orientation variability from the analysis of the covariance of the diffusion tensors. The results showed a strong coherence within the canine population. Thanks to the exceptional access to an ex vivo human cardiac DT-MRI data set, its comparison with the canine population showed good interspecies similarities [30]. The use of an average model from different species makes sense for a more realistic and generic prior knowledge on fiber orientations. Because it is known that some pathologies have an impact on the fiber architecture, there may be local adjustment to perform on these orientations when simulating these pathologies. This could be done, for example, with synthetic models built with analytic laws describing general trends of fiber orientations observed in different studies [31]. However, the influence of this variability in terms of the electrical and mechanical behavior of the heart is currently studied based on biomechanical simulations.

Myocardial electrophysiology

Electrophysiology model

Modeling the cell electrophysiology (EP) has been an active research area since the seminal work of Hodgkin and Huxley [32]. At the organ level, it involves a cell membrane model embedded into a set of PDEs representing a continuum. The approaches can be divided into three categories, in decreasing order of computational complexity:

- Biophysical: semilinear evolution PDE with ionic models (up to 50 equations for ions and channels) [33–37]
- Phenomenologic: semilinear evolution PDE with mathematical simplifications of biophysical models (bidomain, monodomain) [38–40]

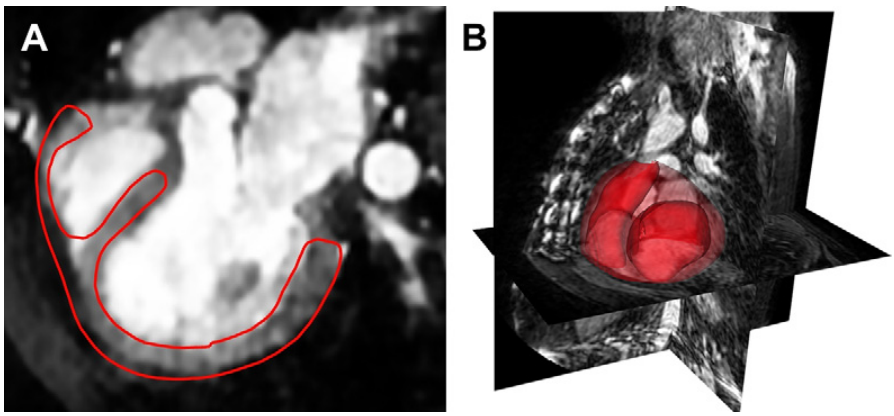

Fig. 4. Results of myocardium segmentation using the presented pipeline. (*A*) Intersection between the final segmentation (*in red*) and the MR image. (*B*) 3D visualization of the final mesh within the MR volume.

Author's personal copy

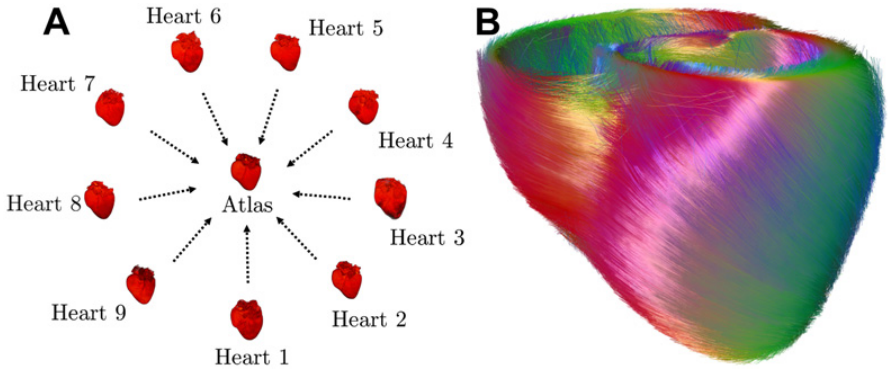

Fig. 5. Statistical atlas of cardiac fibers architecture. (*A*) A groupwise registration of the cardiac geometries to an average geometry. (*B*) Fiber tracking performed with the average DT-MRI.

- Eikonal: one static nonlinear PDE for the depolarization time derived from the previous models (Eikonal-curvature, Eikonal-diffusion) [41,42].

Solutions of the evolution PDE are computationally very demanding, because of the space scale of the electrical propagation being much smaller than the size of the ventricles, and the stability issues of the dynamic aspect. The Eikonal equation is static and the front can be observed at a larger scale, resulting in much faster computations.

For the authors' clinical applications, very fast models that can be adjusted to the data must be designed. Moreover, meaningful clinical data currently available reliably describes the propagation times, but are not suited for accurate estimation of extracellular or action potentials. For these reasons, the authors chose to base their work on the Eikonal models. Even if these models may not be able to precisely simulate the complete range of cardiac pathologies, they open up possibilities for fast parameter estimation, as well as data filtering, interpolation, and extrapolation.

An anisotropic multifront, fast marching method was developed to solve the Eikonal model equations very efficiently [43]. The Eikonal model is capable of simulating complex depolarization wavefront rotations around functional blocks. The authors base their model on the Eikonal diffusion (ED) equation. The static ED equation for the depolarization time (T_d) in the myocardium is given by

$$c_0\sqrt{D}\left(\sqrt{\nabla T_d^t \mathbf{M} \nabla T_d}\right) - (D\nabla \cdot \mathbf{M}\nabla T_d) = \tau \quad (1)$$

where c_0 is a dimensionless constant related to the cell membrane, τ is the cell membrane time constant, and D is the square of the membrane space constant and thus related to the volumetric electrical conductivity of the tissue. The tensor quantity relating to the fiber directions is given by $\mathbf{M} = \mathbf{A}\overline{D}\mathbf{A}^t$, where A is the matrix defining the fiber directions in the global coordinate system and $\overline{D} = \mathrm{diag}(1, \lambda^2, \lambda^2)$. In this equation, λ is the anisotropic ratio of membrane space constants along and transverse to the fiber direction and is of the order 0.4 in human myocardium (see Ref. [44] for more details on the ED equation and its parameters).

Patient-specific electrophysiology

To personalize the electrophysiology model, the authors propose to estimate the cardiac cell membrane space constant (D) in the Eikonal model, which corresponds to an apparent conductivity (AC). The idea is to estimate the AC by matching the simulated propagation times of the model to clinically measured propagation times of the patient. Once this process has been achieved, a patient-specific electrophysiology model can be realized, which can help in diagnosis and therapy planning. The EP model adjustment procedure is divided into two components:

- A nominal value of the AC is estimated by minimizing the average difference between the simulated and measured depolarization times using a bisection method. This step enables the simulated and measured propagation times to be brought to the same scale.
- A multilevel approach is then taken by adaptively subdividing the entire region of the endocardium into zones where the AC on each zone is estimated using a least-squares approach and modified Brent minimization algorithm.

The authors present the application of the EP model adjustment algorithm to build a

Author's personal copy

patient-specific EP model for a clinical case with left bundle branch block pathology. The patient underwent electrophysiology study in the XMR environment where an Ensite array (St. Jude Medical) is inserted into the left ventricle via a retrograde aortic approach. The baseline (normal sinus rhythm) propagation times were measured by the Ensite array and are used to adjust the Eikonal model for this particular patient (Fig. 6).

Once the EP model has been adjusted to a particular patient data, the model can then be used in its predictive capacity. Fig. 7 shows how the adjusted EP model can be used to predict a propagation map from a different pacing site. Fig. 7B presents the application of the adjusted model to predict the isochrones of propagation when paced from a postero-lateral position in the endocardium. By comparing these isochrones with those measured during pacing (Fig. 7A), it can be seen that this adjusted model can indeed be a first step toward the development of a patient specific EP model. Such models could be very useful, for example, for the planning of multisite cardiac stimulation, as used for the treatment of patients with ventricular asynchrony.

Furthermore, an additional conduction related parameter, the conduction velocity (v_{app}), can be estimated from the apparent conductivity parameter: $v_{app} = c_0\sqrt{D}/\tau$. These conduction velocity maps can aid in determining possible scars, as they show up as areas of low conduction velocity on these velocity maps. Fig. 8 shows such a resultant conduction velocity map obtained for a different clinical case after EP model adjustment. This patient had scars caused by an earlier myocardial infarction. From the figures, it can be seen from the adjusted conductivity parameter colormap, that areas of low conduction velocity (black regions on the endocardial surface) do correspond to the scar locations, as obtained by the segmentation of the late-enhancement images.

Myocardial biomechanics

Constitutive law of the myocardium

The myocardium is an active nonlinear anisotropic visco-elastic material. Its constitutive law is complex and includes an active part for contraction, controlled by the transmembrane potential propagation (which can be computed from the previous section), and a passive part representing the mechanical elasticity of the myocardium. Several constitutive laws have been proposed in the literature [45–51]. These laws are designed to precisely fit rheologic tests made on in vitro cardiac muscle.

Another approach is to model contraction from the nanomotors scale and build up a macroscopic constitutive law representing the phenomena encountered at the different scales, which is the approach followed by Bestel-Clément-Sorine [52]. A detailed study of this complex model and simulations can be found in the work of Sainte-Marie and colleagues [53] and Moireau and colleagues [54]. This model is based on the Hill-Maxwell scheme.

The electromechanical model used here was motivated by the multiscale and phenomenologic approach of Bestel-Clément-Sorine, but it is

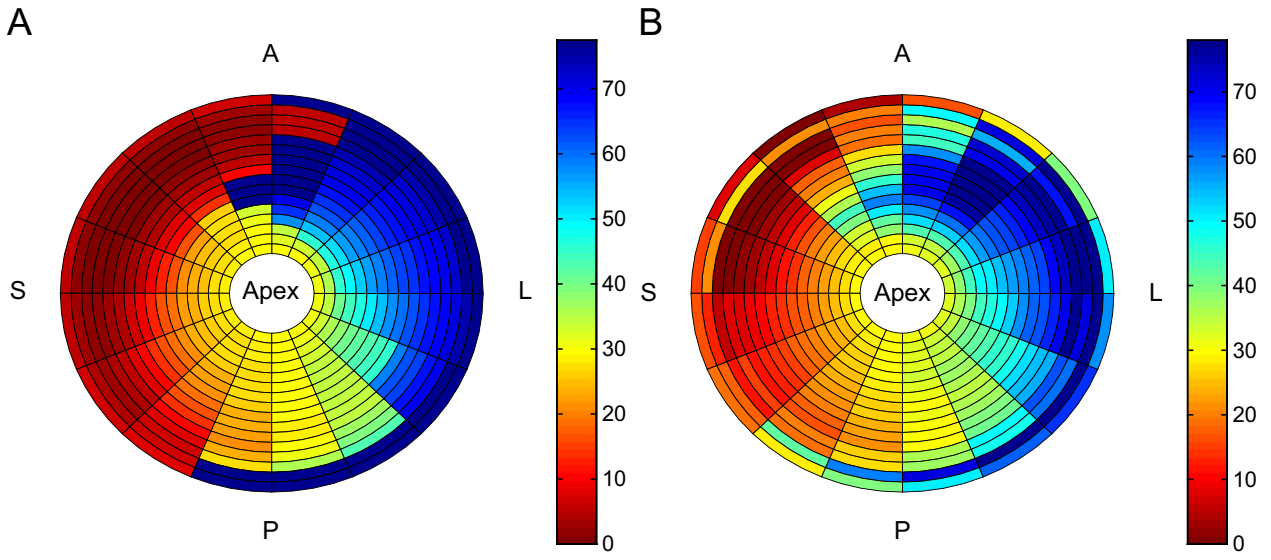

Fig. 6. Bull's-eye plots of depolarization times from a patient with left bundle branch block. (*A*) Measured isochrones using Ensite during sinus rhythm. (*B*) Simulated isochrones with the adjusted electrophysiology model.

Author's personal copy

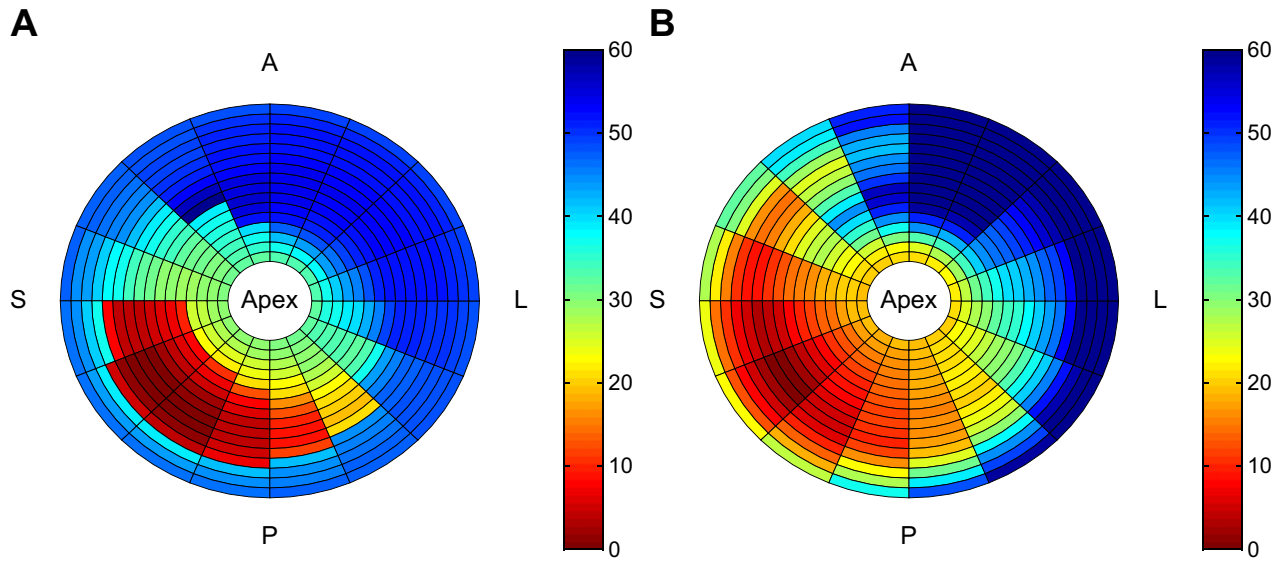

Fig. 7. Usage of the adjusted EP model to predict propagation map from a different pacing site. (*A*) Measured isochrones using Ensite during pacing. (*B*) Isochrones of depolarization predicted by the adjusted electrophysiology model.

specifically designed for cardiac image analysis and simulation. It is built to be computationally efficient and with few parameters directly related to clinical parameters, so the authors chose to simplify the constitutive law of the Bestel-Clément-Sorine approach. The simplified mechanical model has the following components:

- An active contractile element, which creates a stress tensor σ_c, controlled by the command u, depending on the depolarisation time T_d and repolarisation time T_r;
- A passive parallel element which is anisotropic linear visco-elastic and creates a stress tensor σ_p.

For the electromechanical coupling, several different laws have also been proposed [45,49]. The authors believe that it is important to keep the model simple, as relatively few clinical

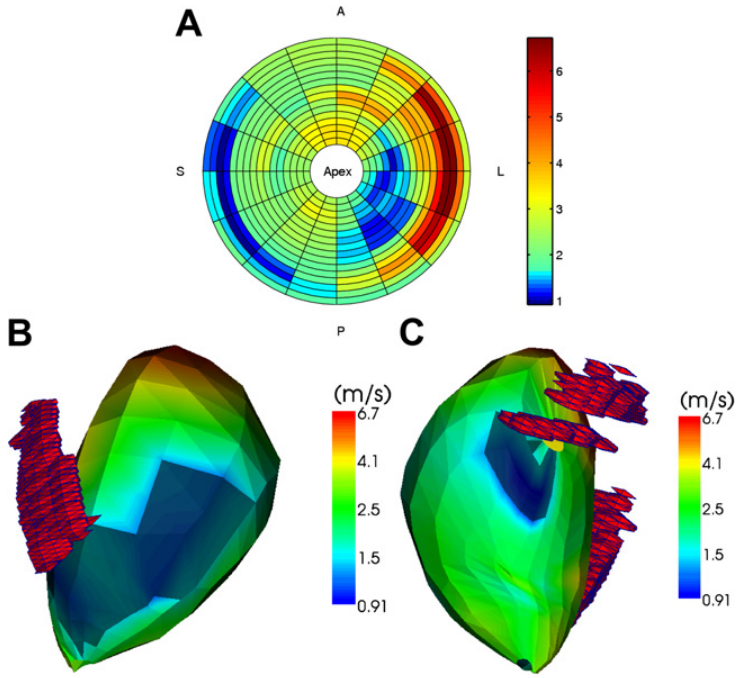

Fig. 8. (*A*) Estimated conduction velocity, where scars appear as small value regions (*blue*). (*B,C*) Areas of slow conduction (*black regions*) after EP model adjustment, compared with scar locations obtained from late-enhancement MRI image (*red wire-meshes*).

Author's personal copy

measures are available to adjust it. The contraction of a heart muscle cell (like all muscle cells) is controlled by cycling levels of calcium, which are stored in the sarcoplasmic reticulum. When depolarization occurs, the concentration of calcium increases in the cytosol and allows the adenosine diphosphate (ATP) hydrolysis, which provides energy to the molecular motors in the sarcomeres, generating the contraction of the fiber. The command u is then equal to a constant k_{ATP}, which represents the rate of the hydrolysis of the ATP. After contraction, during the depolarization, calcium moves back from the cytosol into the sarcoplasmic reticulum, and this calcium decrease leads to the relaxation of the muscle. The command u is then equal to another constant ($-k_{RS}$), which models the activity of the sarcoplasmic reticulum. The simplest way to model this contractile element is thus through an ordinary differential equation of the type $\dot{\sigma}_c + |u|\sigma_c = |u|_+\sigma_0$, with $\dot{\sigma}_c$ the time derivative of σ_c, σ_0 the maximum intensity of the contractionand, and $|u|_+$ the positive part of the command u, equal to u if u is greater than or equal to 0 and 0 if not. With this equation, the authors obtain the following coupling model (Equation 2 below), with T_d the depolarization time, T_r the depolarization time, HP the heart period, and $\sigma_r = \sigma_c(T_r)$.

The constants k_{ATP} and k_{RS} allow the contraction stress increase and decrease to be controlled, which is consistent with their precedent definition. A time delay between the electrical and the mechanical phenomena in this coupling can also be added. The command and the resulting contraction are represented in Fig. 9.

To numerically simulate this simplified constitutive law, the authors use the finite element method on a tetrahedral mesh to solve the discretised dynamics equation: $M\ddot{U} + C\ddot{U} + KU = F_b + F_c$, with U the displacement vector, M the mass matrix, C the damping matrix for the internal viscosity part, K the stiffness matrix for the transverse anisotropic elastic part (parallel element), F_c the force vector computed from contraction (contractile element), and F_b the different external loads from the boundary conditions, detailed in the following section.

Boundary conditions: the cardiac phases

To simulate a whole cardiac cycle, the interaction of the myocardium with the blood is crucial. The cardiac cycle has four different phases (filling, isovolumetric contraction, ejection, isovolumetric relaxation), which implies different boundary conditions:

- Filling: the preload pressure is applied to the endocardium. Its intensity is equal to the pressure of the atrium. It is augmented during the P wave to represent atrial contraction. When the ventricular contraction starts, the contraction force will tend to eject blood, so when this force becomes more important than the applied pressure, the blood flow changes sign. As the blood is considered incompressible, the conservation of mass allows the computation of blood flow directly with the ventricular volume time derivative. This is used to close the atrial-ventricular valves and start the isovolumetric contraction.
- Isovolumetric contraction: the ventricular pressure computed to counterbalance the contraction force and then to keep the ventricle volume constant is applied to the vertices of the endocardium. When the ventricular pressure is more important than the arterial pressure, the ventricular-arterial valves open, and the ejection phase starts.
- Ejection: a pressure is applied to the vertices of the endocardium. Its intensity is equal to the pressure of the aorta (for the left ventricle) and the pulmonary artery (for the right ventricle). Contraction force decreases after repolarization. When the flow changes sign, the ventricular-arterial valves close, starting the isovolumetric relaxation phase.
- Isovolumetric relaxation: the ventricular pressure computed to keep the ventricular volume constant is applied to the vertices of the endocardium. When the ventricular pressure is less important than atrial pressure, the atrial-ventricular valves open, starting the filling phase.

The efficient implementation of such changing boundary conditions is an important part of

$$\begin{cases} \text{if } T_d \le t \le T_r : \ \sigma_c(t) = \sigma_0\left(1 - e^{k_{ATP}(T_d - t)}\right) \text{ as } \dot{\sigma}_c + k_{ATP}\sigma_c = k_{ATP}\sigma_0 \\ \text{if } T_r < t < T_d + HP : \ \sigma_c(t) = \sigma_r e^{k_{RS}(T_r - t)} \text{ as } \dot{\sigma}_c + k_{RS}\sigma_c = 0 \end{cases} \quad (2)$$

Author's personal copy

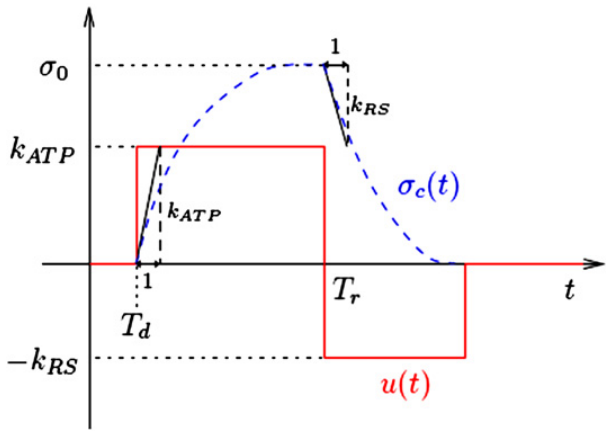

Fig. 9. Command $u(t)$ and contraction $\sigma_c(t)$ generated.

achieving fast enough mechanical simulations. In the model by Sermesant and colleagues [55], a penalty constraint was applied to the vertices of the endocardium to keep its volume constant. To achieve a balance between this constraint and the contraction, very small time steps had to be used. The authors now use the constrained optimization theory to directly compute the ventricular pressure, keeping the volume constant. The authors minimize the energy of the mechanical system of the heart $J(U) = \frac{1}{2}(U^t \tilde{K} U - U^t \tilde{F})$ under the constraints $V = V^\circ$, with V the volume in the considered ventricle (depending on U) and V° its volume at the beginning of the isovolumetric phase. $\tilde{K}$ and $\tilde{F}$ are two matrices obtained by a first integration of the dynamics equation. The pressure forces are contained in the $\tilde{F}$ matrix. At each time step, the authors compute the ventricular pressure for which the solution U of the above constrained minimization system is such that the volume is kept constant. This method can sustain much larger time steps (100 times greater than before), which allows the authors to simulate a whole heartbeat on a mesh with 50,000 elements in about 5 minutes on a standard computer. This improvement opens up possibilities in mechanical parameter adjustment and allows the behavior of the model on series of beats to be tested.

Despite its simplicity when compared with other constitutive laws proposed in the literature, this model reproduces reasonably well the global and local behavior of the myocardium. Fig. 10 shows the simulation of this model using the canine cardiac atlas for the myocardial shape and fiber structure.

In the current implementation, the atria pressures vary smoothly between two values (baseline

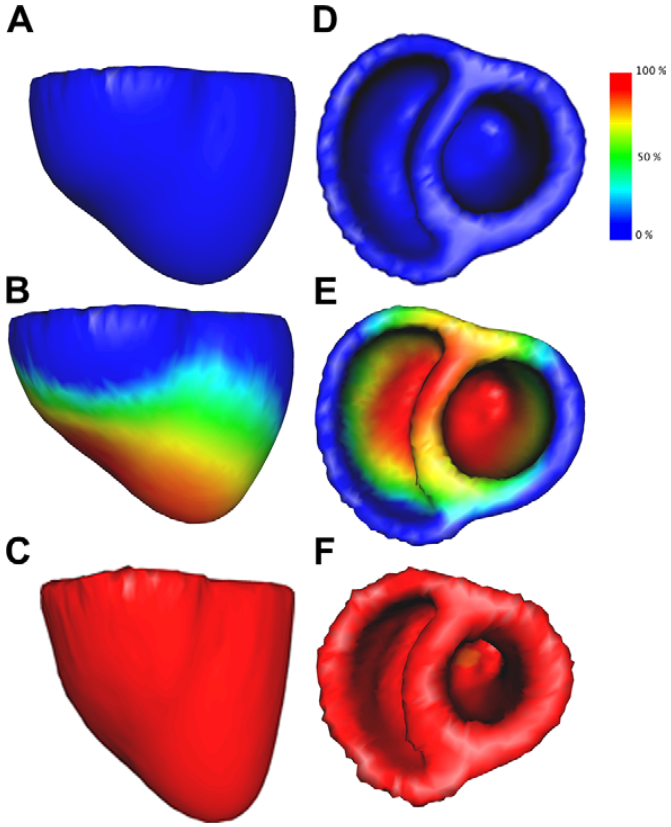

Fig. 10. Long axis and short axis views of the heart model at different phases of the heart cycle. (*A–F*) Colors represent the intensity of the contraction stress.

Author's personal copy

and atrial systolic pressure). The authors use a three-element Windkessel model to compute the arterial pressures from the arterial flow. Windkessel models are derived from electrical circuit analogies, where current and voltage represent arterial flow and pressure, respectively, and have been found to represent well (after proper adjustment of the parameters) the clinical measurements [56–58]. To hold the mesh in space, the authors simulate the fibrous structure around the valves with springs, having one extremity attached to a basal node and the other extremity attached to a fixed point. Some simulation outputs are presented in Fig. 11.

The authors can note that even with these completely independent conditions for the left and right parts of the heart, the two ventricles stay well synchronized, which shows that force development is coherent in the model. It allows calibration of the contractility parameters σ_0, k_{ATP}, and k_{RS} from the duration of the different phases, and also from the atrial and arterial pressures, before further local adjustment, using, for example, cine-MRI.

Toward patient-specific simulations

Preliminary simulations of patient heart function are already possible through this framework. Right-ventricle overload caused by congenital heart diseases, for example, can be simulated to study the effect of the abnormal myocardium anatomy and loading conditions upon the cardiac function.

To illustrate the overall framework, the authors present the adjustment of the electromechanical model to a patient with Tetralogy of Fallot. The myocardium shape is extracted from the patient image data using the presented segmentation pipeline. The biomechanical parameters are manually calibrated: maximum contraction σ_0 is obtained by comparing the simulated and real diameters of the ventricles at end-systole; contraction rate k_{ATP} and relaxation rate k_{RS} are estimated using both the dynamic images and the volume diagrams obtained from the segmentations. Because they are not accessible for this patient, electrical parameters and boundary conditions are set according to clinical observations available in the literature.

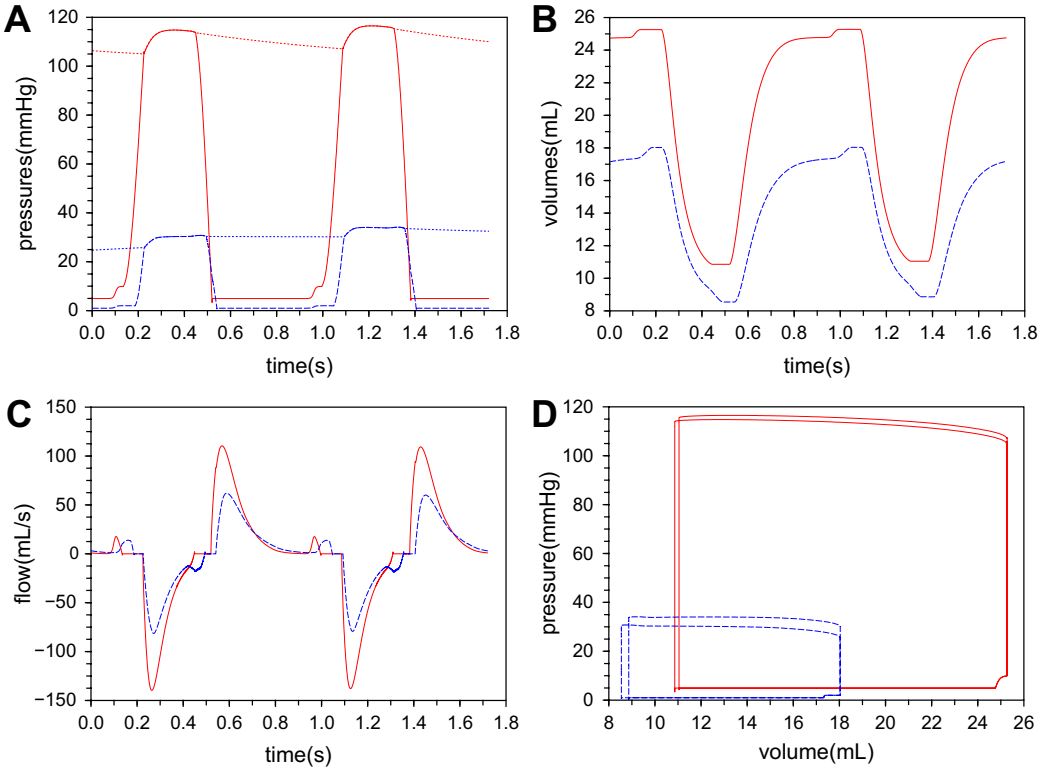

Fig. 11. (*A*) Ventricular, aorta and pulmonary artery pressures (in mm Hg). (*B*) Ventricular volumes (in mL). (*C*) Flows (in mL/mn). (*D*) Pressure-Volume cycles. The dash (and red) curves and the solid (and blue) curves represent respectively the right and the left ventricles. The dot curves in (*A*) represent the aorta and the pulmonary artery pressures.

Author's personal copy

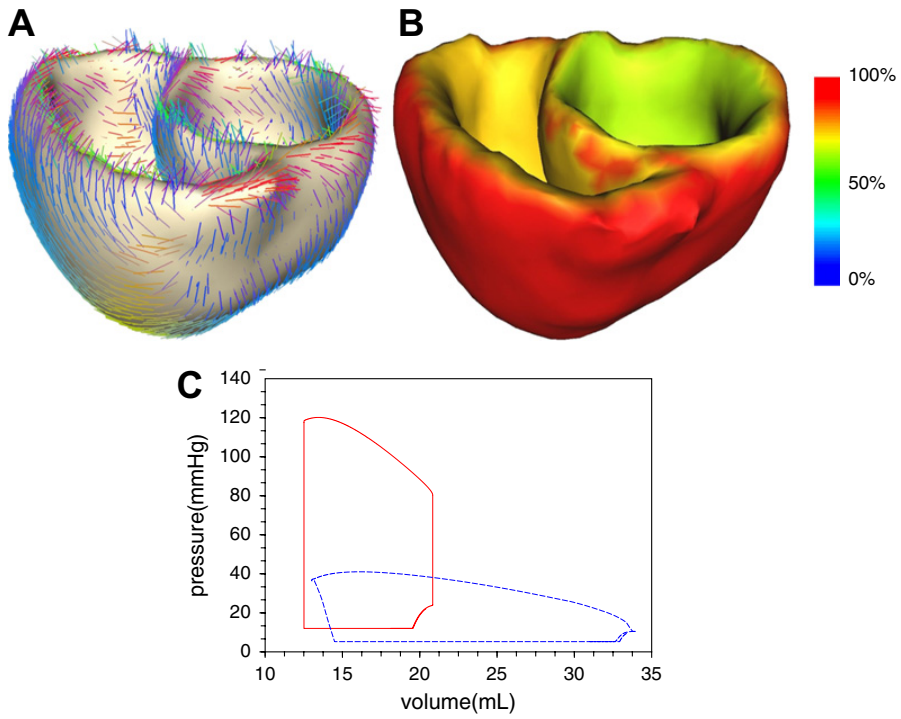

Fig. 12. (*A*) Anatomy of the right-ventricle overload patient with synthetic fiber orientations. (*B*) Contraction of the model: end-systole position; colors represent the contraction stress. (*C*) Pressure-volume loops, demonstrating right ventricle enlargement and regurgitations.

The left ventricle can be simulated successfully, as well as the regions of the right ventricle far from the outflow tract. The simulated contraction at each vertex of the mesh, the electrical propagation, and the 3D strain can be visualized in real time to assess the cardiac function (Fig. 12). Additional results on this disease-adapted work can be found on the World Wide Web (http://www-sop.inria.fr/asclepios/projects/hec/).

However, the abnormal regions of the right ventricle are still difficult to simulate because of some limitations in the model: in particular the authors' way of handling the fluid-structure interactions, which may not be suited to these pathologies. The authors introduced here a preliminary model of valve regurgitation, which is an important feature of this pathology; however, local abnormalities also have to be introduced in the model parameters to better represent the diseased behavior.

In summary, this article presents a framework toward patient-specific models of the myocardium. By integrating information about the anatomy, the electrophysiology, and the mechanics, we can explore the correlation between function and anatomy for a given patient and test different hypothesis as well as plan therapies.

To complete the personalization of the model, the parameters of the mechanical model must be adjusted locally, as was presented on the electrophysiology model. First results have been obtained on this problem, using the data assimilation framework of Sermesant and colleagues [59], but this is still very challenging. One of the additional difficulties, compared with the electrophysiology, is to precisely know the boundary conditions, such as the before-load and the after-load. In addition, the mechanical behavior depends on the electrophysiology, which is the command. Then, if errors were to occur in the electrophysiology model adjustment, this would lead to errors in the mechanical parameter adjustment. Thus, the progress made on the data acquisition and fusion will definitely play an important role in achieving a fully patient-specific heart model.

References

[1] MacLeod R, Yilmaz B, Taccardi B, et al. Direct and inverse methods for cardiac mapping using multielectrode catheter measurements. Journal of Biomedizinische Technik 2001;46:207–9.

[2] Faris O, Evans F, Ennis D, et al. Novel technique for cardiac electromechanical mapping with magnetic resonance imaging tagging and an epicardial electrode sock. Ann Biomed Eng 2003;31(4):430–40.

Author's personal copy

[3] Masood S, Yang G, Pennell D, et al. Investigating intrinsic myocardial mechanics: the role of MR tagging, velocity phase mapping and diffusion imaging. J Magn Reson Imaging 2000;12(6):873–83.
[4] Kilner P, Yang G, Wilkes A, et al. Asymmetric redirection of flow through the heart. Nature 2000; 404:759–61.
[5] McCulloch A, Bassingthwaighte J, Hunter P, et al. Computational biology of the heart: from structure to function. Prog Biophys Mol Biol 1998;69(2–3): 151–559.
[6] Hunter P, Pullan A, Smaill B. Modeling total heart function. Annu Rev Biomed Eng 2003;5:147–77.
[7] Xia L, Huo M. Analysis of ventricular wall motion based on an electromechanical biventricular model. In: Murray A, editor. Computers in cardiology. New York: IEEE; 2003. p. 315–8.
[8] Noble D. Modeling the heart. Physiology (Bethesda) 2004;19:191–7.
[9] Nickerson D, Nash M, Nielsen P, et al. Computational multiscale modeling in the IUPS physiome project: modeling cardiac electromechanics. Systems Biology 2006;50(6):617–30.
[10] Rhode K, Sermesant M, Brogan D, et al. A system for real-time XMR guided cardiovascular intervention. IEEE Trans Med Imaging 2005;24(11):1428–40.
[11] Frangi A, Niessen W, Viergever M. Three-dimensional modeling for functional analysis of cardiac images: a review. IEEE Trans Med Imaging 2001; 1(20):2–25.
[12] Frangi A, Rueckert D. Duncan J. editors. New trends in three-dimensional cardiac image analysis. Vol. 21(9). IEEE Transactions on Medical Imaging. New York: IEEE.
[13] Montagnat J, Delingette H. 4D deformable models with temporal constraints: application to 4D cardiac image segmentation. Med Image Anal 2005;9(1): 87–100.
[14] Kaus M, von Berg J, Weese J, et al. Automated segmentation of the left ventricle in cardiac MRI. Med Image Anal 2004;8(3):245–54.
[15] Papademetris X, Sinusas A, Dione D, et al. Estimating 3D left ventricular deformation from 3D medical image sequences using biomechanical models. IEEE Trans Med Imaging 2002;21(7):786–800.
[16] Bistoquet A, Oshinski J, Skrinjar O. Left ventricular deformation recovery from cine MRI using an incompressible model. IEEE Trans Med Imaging 2007;26(9):1136–53.
[17] Linte A, Wierzbicki M, Moore J, et al. Towards subject-specific models of the dynamic heart for image-guided mitral valve surgery. In: Ayache N, Ourselin S, Maeder A, editors. Medical image computing and computer-assisted intervention. Berlin: Springer-Verlag; 2007. p. 94–101.
[18] Lorenzo-Valdes M, Sanchez-Ortiz GI, Elkington AG, et al. Segmentation of 4D cardiac MR images using a probabilistic atlas and the EM algorithm. Med Image Anal 2004;8(3):255–65.
[19] Peters J, Ecabert O, Meyer C, et al. Automatic whole heart segmentation in static magnetic resonance image volumes. In: Ayache N, Ourselin S, Maeder A, editors. Medical image computing and computer-assisted intervention. Berlin: Springer-Verlag; 2007. p. 402–10.
[20] van Assen HC, Danilouchkine MG, Frangi AF, et al. SPASM: a 3D-ASM for segmentation of sparse and arbitrarily oriented cardiac MRI data. Med Image Anal 2006;10(2):286–303.
[21] von Berg J, Lorenz C. Multi-surface cardiac modeling, segmentation, and tracking. In: Frangi A, Radeva P, Santos A, et al, editors. Functional imaging and modeling of the heart. Berlin: Springer-Verlag; 2005. p. 1–11.
[22] Sermesant M, Forest C, Pennec X, et al. Deformable biomechanical models: application to 4D cardiac image analysis. Med Image Anal 2003;7(4):475–88.
[23] Sled JG, Zijdenbos AP, Evans AC. A nonparametric method for automatic correction of intensity nonuniformity in MRI data. IEEE Trans Med Imaging 1998;17(1):87–97.
[24] Weickert J, ter Haar Romeny BM, Viergever MA. Efficient and reliable schemes for nonlinear diffusion filtering. IEEE Trans Image Process 1998;7(3): 398–410.
[25] Lorensen WE, Cline HE. Marching cubes: a high resolution 3D surface construction algorithm. In: Stone M, editor. SIGGRAPH'87: Proceedings of the 14th annual conference on Computer graphics and interactive techniques, vol. 21. New York: ACM Press; 1987. p. 163–9.
[26] Turk G, O'Brien J. Variational implicit surfaces. Technical report, Georgia Institute of Technology; 1999.
[27] Tseng W-YI, Reese TG, Weisskoff RM, et al. Cardiac diffusion tensor MRI in vivo without strain correction. Magn Reson Med 1999;42(2):393–403.
[28] Nielsen P, Grice IL, Smail B, et al. Mathematical model of geometry and fibrous structure of the heart. Am J Physiol Heart Circ Physiol 1991;260(29): H1365–78.
[29] Hsu EW, Muzikant AL, Matulevicius SA, et al. Magnetic resonance myocardial fiber-orientation mapping with direct histological correlation. Am J Physiol Heart Circ Physiol 1998;274:H1627–34.
[30] Peyrat J-M, Sermesant M, Pennec X, et al. A computational framework for the statistical analysis of cardiac diffusion tensors: Application to a small database of canine hearts. IEEE Trans Med Imaging 2007;26(11):1500–14.
[31] Streeter D. Handbook of physiology. In: Berne R, Sperelakis N, editors. The cardiovascular system: gross morphology and fiber geometry of the heart. Baltimore (MD): Williams & Wilkins; 1979.
[32] Hodgkin A, Huxley A. A quantitative description of membrane current and its application to conduction and excitation in nerve. J Physiol 1952;177:500–44.

Author's personal copy

[33] Noble D. A modification of the Hodgkin–Huxley equations applicable to Purkinje fibre action and pace-maker potentials. J Physiol 1962;160:317–52.
[34] Beeler GW, Reuter H. Reconstruction of the action potential of ventricular myocardial fibers. J Physiol 1977;268:177–210.
[35] Luo C, Rudy Y. A model of the ventricular cardiac action potential: depolarization, repolarization, and their interaction. Circ Res 1991;68:1501–26.
[36] Noble D, Varghese A, Kohl P, et al. Improved guinea-pig ventricular cell model incorporating a diadic space, I_{Kr} and I_{Ks}, and length and tension dependent processes. Can J Cardiol 1998;14:123–34.
[37] Ten Tusscher K, Noble D, Noble P, et al. A model of the human ventricular myocyte. Am J Physiol Heart Circ Physiol 2004;286(4):1573–89.
[38] FitzHugh R. Impulses and physiological states in theoretical models of nerve membrane. Biophys J 1961;1:445–66.
[39] Pollard A, Hooke N, Henriquez C. Cardiac propagation simulation. Crit Rev Biomed Eng 1992; 20(3,4):171–210.
[40] Aliev R, Panfilov A. A simple two-variable model of cardiac excitation. Chaos Solitons Fractals 1996; 7(3):293–301.
[41] Keener J, Sneyd J. Mathematical physiology. New York: Springer; 1998.
[42] Colli Franzone P, Guerri L, Rovida S. Wavefront propagation in activation model of the anisotropic cardiac tissue: asymptotic analysis and numerical simulations. J Math Biol 1990;28(2):121–76.
[43] Sermesant M, Konukoglu E, Delingette H, et al. An anisotropic multi-front fast marching method for real-time simulation of cardiac electrophysiology. In: Sachse F, Seemann G, editors. Proceedings of functional imaging and modeling of the heart. Vol 4466. Berlin: Springer-Verlag; 2007. p. 160–9.
[44] Tomlinson K. Finite element solution of an Eikonal equation for excitation wavefront propagation in ventricular myocardium, Ph.D. thesis, University of Auckland (2000).
[45] Hunter P, Smaill B. The analysis of cardiac function: a continuum approach. Prog Biophys Mol Biol 1988;52:101–64.
[46] Humphrey J, Strumpf R, Yin F. Determination of a constitutive relation for passive myocardium: I. A new functional form. J Biomech Eng 1990;112: 333–9.
[47] Guccione J, McCulloch A. Theory of heart: biomechanics, biophysics, and nonlinear dynamics of cardiac function. In: Glass L, Hunter PJ, McCulloch AD, editors. Finite element modeling of ventricular mechanics. New York: Springer-Verlag; 1991. p. 121–44.
[48] Hunter P, Nash M, Sands G. Computational biology of the heart. In: Panfilov A, Holden A, editors. Computational electromechanics of the heart. West Sussex (UK): John Wiley & Sons; 1997. p. 345–407.
[49] Nash M. Mechanics and material properties of the heart using an anatomically accurate mathematical model. Ph.D. thesis. University of Auckland; 1998.
[50] Häfner J, Sachse F, Sansour C, et al. Hyperelastic description of elastomechanic properties of the heart: A new material law and its application. Biomed Tech (Berl) 2002;47(1–2):770–3.
[51] Caillerie D, Mourad A, Raoult A. Cell-to-muscle homogenization. Application to a constitutive law for the myocardium. Mathematical Modelling and Numerical Analysis 2003;37(4):681–98.
[52] Bestel J. Clément F. Sorine M. A biomechanical model of muscle contraction. In: Niessen W, Viergever M, editors. Medical image computing and computer-assisted intervention. Vol 2208. Lecture Notes in Computer Science (LNCS). Berlin: Springer-Verlag; 2001. p.1159–61.
[53] Sainte-Marie J, Chapelle D, Cimrman R, et al. Modeling and estimation of the cardiac electromechanical activity. Comput Struct 2006;84:1743–59.
[54] Moireau P, Chapelle D, Le Tallec P. Joint state and parameter estimation for distributed mechanical systems. Computer Methods in Applied Mechanics and Engineering 2008;197:659–77.
[55] Sermesant M, Delingette H, Ayache N. An electromechanical model of the heart for image analysis and simulation. IEEE Trans Med Imaging 2006; 25(5):612–25.
[56] MacDonald A. Blood flow in the arteries. London: Edward Arnold; 1974.
[57] Stergiopulos N, Westerhof B, Westerhof N. Total arterial inertance as the fourth element of the Windkessel model. Am J Physiol 1999;276:H81–8.
[58] Muthurangu V, Atkinson D, Sermesant M, et al. Measurement of total pulmonary arterial compliance using invasive pressure monitoring and MR flow quantification during MR-guided cardiac catheterization. Am J Physiol Heart Circ Physiol 2005;289(3):1301–6.
[59] Sermesant M, Moireau P, Camara O, et al. Cardiac function estimation from MRI using a heart model and data assimilation: advances and difficulties. Med Image Anal 2006;10(4):642–56.